Crevice Corrosion of Grade-2 Titanium in Saline Solutions at Different Temperatures and Oxygen Concentrations

Thalia E. Standish,* Mehdi Yari, David W. Shoesmith, and James J. Noël***,z**

Department of Chemistry and Surface Science Western, The University of Western Ontario, London, Ontario N6A 5B7, Canada

Titanium alloys are candidate materials for the fabrication of high level nuclear waste containers but may be susceptible to crevice corrosion in the initial warm oxidizing conditions anticipated in a deep geological repository. The crevice corrosion of Grade-2 titanium has been studied in 1.0 mol/L NaCl at various temperatures (120°C and 150°C) and oxygen concentrations using a galvanic coupling technique. The current due to propagation supported by oxygen reduction on the surface external to the crevice was monitored electrochemically and the total propagation determined from weight change measurements. The redistribution of impurities (Fe, V, Mo) during corrosion was determined by dynamic secondary ion mass spectrometry. Propagation was dominantly driven by the reduction of protons created inside the crevice by cation hydrolysis. Damage accumulated at the locations of Ti_xFe intermetallic particles, which are both anodically reactive and function as catalytic cathodes for proton reduction. The compact $TiO_2 \cdot xH_2O$ deposits at active sites led to stifling of corrosion when only between 9 and 56% of the available oxygen had been consumed. While propagation was more rapid at 150°C than at 120°C, it was more readily stifled at the higher temperature, leading to the accumulation of less damage.

 [DOI: 10.1149/2.0941713jes]

Manuscript submitted June 9, 2017; revised manuscript received October 2, 2017. Published October 17, 2017.

Titanium is used in a wide range of applications due to its light weight, superior mechanical properties, and its excellent corrosion resistance, and is considered as a candidate material for the fabrication of engineered barriers for the permanent disposal of high level nuclear waste in a deep geological repository (DGR).[1–4] The anticipated degradation mechanisms for Ti engineered barriers that could lead to their eventual failure are; (a) crevice corrosion and (b) general corrosion leading to hydrogen-induced cracking (HIC).[2–4] Of these degradation mechanisms, crevice corrosion offers the most serious threat of early failure, unless expensive alloying additions are made. This is a concern since the required occluded conditions could exist on container surfaces in contact with solid backfill materials or under deposits formed as exposure conditions evolve.

In most DGRs considered internationally, conditions are expected to be saline and to evolve from initially warm and oxidizing to eventually cool and anoxic, with the exact conditions determined by the DGR design and location and the characteristics of the heat-producing wasteform within the containers. Consequently, if crevice corrosion is to occur, it will initiate during the early warm oxidizing period, since, in aqueous chloride solutions, the protective oxide on Ti is known to be destabilized by recrystallization at temperatures $\geq 70°C$.[5] Once initiated, acidic conditions are rapidly established within the occluded region, as illustrated schematically in Figure 1. Although Ti^{4+} is shown as the solution species, the anodic dissolution in the acidic conditions within the crevice occurs as the more soluble Ti^{3+}, which is subsequently converted to the insoluble Ti^{4+} by O_2 reduction on surfaces external to the crevice and deposited locally as hydrated TiO_2.[6] Our previous studies[5] show this conversion is very efficient, with negligible amounts of soluble Ti^{3+} escaping from the occluded region. The anodic dissolution of Ti within the crevice is driven by two cathodic processes; (i) the reduction of dissolved O_2 on external surfaces and (ii) H^+ reduction on internal surfaces. The primary factors which will influence the initiation and propagation of crevice corrosion are the O_2 and Cl^- concentrations, temperatures, alloy composition including impurities, and the physical dimensions of the crevice, in particular the crevice gap.[5,7,8] Our particular interest in this study is to determine how the process of crevice propagation will progress as the exposure environment evolves from hot and oxidizing to cool and anoxic as anticipated in a DGR.

Since the chemistry required to sustain crevice propagation is dictated primarily by the reduction of O_2 at locations external to the crevice, one would intuitively expect that the availability and concentration of O_2 will have the dominant influence on crevice propagation. As a consequence, its eventual exhaustion, as DGR conditions evolve to anoxic, would lead to crevice stifling/repassivation as the production of protons by the hydrolysis of dissolved Ti^{4+} becomes limited and existing protons diffuse out of the crevice, leading to an increase in pH and the reformation of passive oxide.[5,8]

The influence of temperature on crevice corrosion has been studied in some detail. The need for a temperature $\geq 70°C$ to force initiation is well characterized[7,9,10] and it has been shown that if the temperature of an actively propagating crevice is decreased, the propagation rate decreases.[9] For crevice corrosion initiated and propagated at constant temperature, the propagation rate is higher and the duration shorter at higher temperatures.[11] The overall amount of corrosion damage, as determined by weight change, is greater at higher temperatures, even though the consumption of O_2 in the corrosion process is less. This last observation indicates a greater extent of corrosion driven by H^+ reduction within the crevice interior at high temperature, Figure 1.

Small amounts of alloying additions and impurities can dramatically influence crevice behavior.[8] Precious metals (Pt, Pd, Ru) greatly improve the resistance to propagation even when only present in quantities as small as 0.05 to 0.20 wt%.[7] Other alloying elements (e.g., Ni), when present in larger amounts (0.5 to 15 wt%), also enhance resistance to crevice corrosion.[7] The influence of the common impurity Fe is ambiguous and only partly understood, mainly because, even

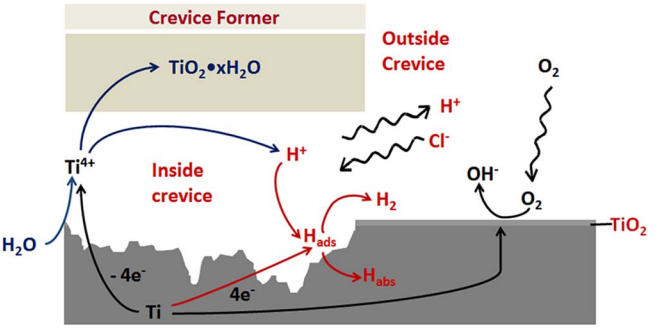

Figure 1. Schematic illustration of the processes involved in the crevice corrosion of titanium.

*Electrochemical Society Student Member.
**Electrochemical Society Fellow.
***Electrochemical Society Member.
zE-mail: jjnoel@uwo.ca

Table I. Elemental composition of commercial Ti-2 alloy plate.

Element	N	O	C	Fe	Ni	Al	V	Mo, Mn, Si, Cr, Cu, Zr, Sn	Ti
Composition (wt%)	0.006	0.146	0.01	0.091	0.02–0.03	0.05	0.03–0.04	<0.01	Bal.
ASTM Grade-2 Ti Standard (wt%)	0.03 max.	0.25 max.	0.08 max.	0.3 max.	-	-	-	*	Bal.

*Other elements: max 0.1 wt% each, 0.4 wt% total.

at the low levels within the allowable range for ASTM Grade-2 Ti, its location within the matrix can either accelerate or retard propagation. When present in the α-Ti hexagonal close packed structure, it is detrimental.[12] However, when segregated into secondary Ti_xFe precipitates, this phase can act as a catalytic site for H^+ reduction within the crevice, thereby leading to repassivation via the well-known cathodic modification effect.[13,14]

In this paper, we have studied the influence of O_2 on crevice propagation of a commercially available Grade-2 Ti (Ti-2) at temperatures of 120°C and 150°C, with the primary goal of determining the distribution of propagation damage and how it is related to these two parameters. In addition, we have tried to demonstrate that repassivation can be achieved when available O_2 is exhausted. Experiments were conducted in 1.0 mol/L NaCl solutions to simulate the saline conditions anticipated in many DGRs.

Experimental

Metallography.—Specimens were cut from plates provided by RMI Titanium Company. The composition is given in Table I. Specimens were prepared for metallographic analyses by mounting in Streurs Epofix resin so that only a single face (area 1 cm^2) was exposed, grinding with 320 grit SiC paper, and polishing with a 9 μm diamond suspension followed by a 0.04 μm colloidal silica suspension. Specimens were then sonicated, first in H_2O, then in acetone, and finally in methanol (cross sections of corroded specimens were prepared in a similar manner).

Metallographic analysis was performed using a LEO (Zeiss) focused ion beam/scanning electron microscope (FIB/SEM).

Electrochemical cell.—Crevice corrosion experiments were conducted using an electrochemical cell built within a Ti pressure vessel to allow experiments at high temperatures while suppressing boiling of the electrolyte solution. The working (creviced) electrode consisted of two pieces of Ti-2 (50 mm × 25 mm × 6.5 mm), fastened through the faces using threaded rods and nuts from the same material, with a 25 mm × 13 mm × 1.6 mm piece of poly(tetrafluoroethylene) (PTFE) sandwiched between them to form a tight crevice. A schematic illustration of the cell is shown in Figure 2, which is described in more detail elsewhere.[9] For crevice corrosion experiments, 600 mL of electrolyte were added to the pressure vessel, leaving ~400 mL of gas headspace. To ensure the inner surfaces of the crevice were wetted, the crevice was assembled in 1 mol/L NaCl solution. The crevices were tightened using a thin PTFE "feeler strip" to ensure a reproducible tightness. The counter electrode was a thin Ti-2 hollow cylinder, 75 mm in diameter and 50 mm in height. A home-made Ag/AgCl (1 mol/L KCl) reference electrode (0.235 V vs. SHE) was used.

Experimental procedure.—Specimens were wet ground with SiC papers up to a 600 grit finish, rinsed with deionized H_2O, sonicated in acetone and rinsed in methanol, dried with Ar, and stored in a desiccator for a minimum of one day. They were then weighed accurately on an analytical balance, with the average of three weighings (within ± 0.1 mg) accepted as the final value.

The 1 mol/L NaCl and 1 mol/L KCl solutions (the latter used in the reference electrode) were prepared using Type-1 ultrapure H_2O (resistivity = 18.2 MΩ · cm) obtained from a Barnstead Nanopure (Thermo Scientific) water purification system. Reagent grade chemicals (Caledon Laboratories, Ltd.) were used.

The pressure vessel was sealed and pressurized to 500 kPa using medical grade N_2 and, depending on the desired [O_2], a certified mixture of either 2.97 vol% O_2/balance N_2 or 10% O_2/balance N_2 (Praxair). These gas compositions allowed the [O_2] to be varied. Low [O_2] (<0.1 vol%) was achieved by evacuating the cell for ~10 min, and then pressurizing with N_2. Pressurizing with 2.97 vol% and 10 vol% O_2 gas mixtures after evacuation established intermediate [O_2]; high [O_2] was achieved by aeration with ambient laboratory air before assembling the vessel and pressurizing with N_2.

The pressure vessel was heated and the crevice current (I_c), crevice electrode potential (E_c), planar electrode potential (E_p), and temperature (T) measured using our own computerized data acquisition software. I_c was measured using a zero resistance ammeter (ZRA) (Keithley 6514 System Electrometer). The use of a counter electrode with a much larger surface area than the non-creviced area of the working electrode (~40:1) ensured that the majority of O_2 reduction (yielding I_c) occurred on the counter electrode, with the contribution from O_2 reduction on the exterior of the creviced electrode introducing an error in our measurement of < 3%. Potentials were measured against the reference electrode using a high impedance voltmeter. Since the reference electrode is located outside the crevice, E_c is the potential at the mouth of the crevice, which will differ from the actual potential at crevice corroding sites. The temperature was measured using a thermocouple inserted in a well in the top of the pressure vessel.

On completion of an experiment, the cell was cooled and the creviced electrode removed, rinsed with Type-1 H_2O and placed in a desiccator for several days. Subsequently, the weight gain due to the accumulation of $TiO_2 \cdot xH_2O$ deposited within the crevice (Figure 1) was taken to be the average of 3 weighings (±0.1 mg). Previous measurements[10] have demonstrated that >99% of the corrosion

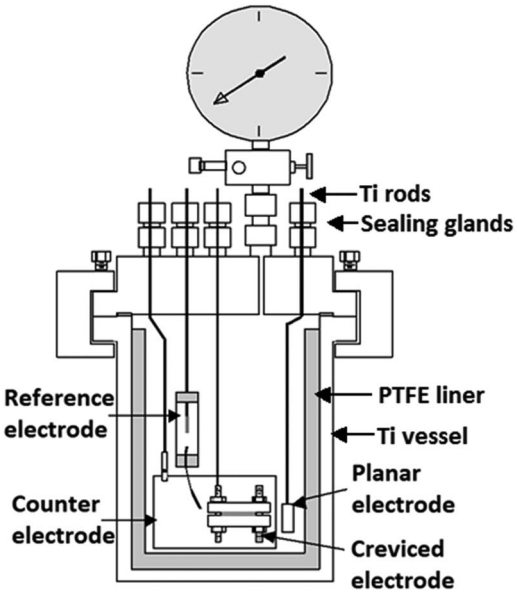

Figure 2. Schematic cross-section of the assembled pressure vessel.

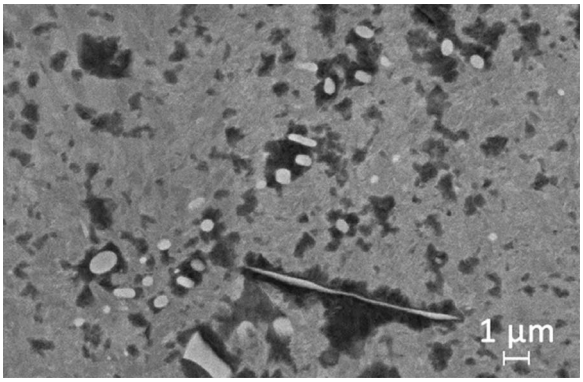

Figure 3. A BSE image of a fine-polished Ti-2 surface.

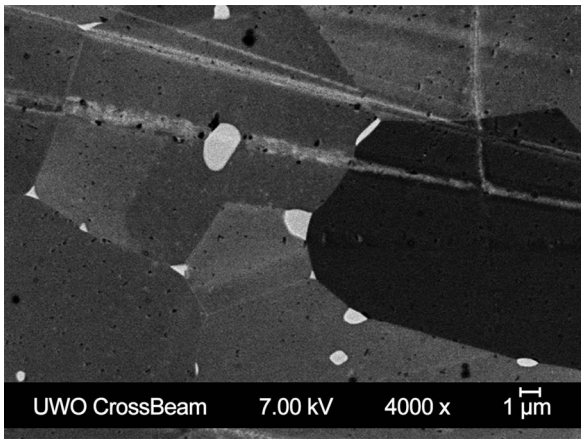

Figure 4. BSE image showing the location of a number of Fe-containing intermetallic particles (white areas).

product is retained in this deposit. The weight gain was converted to an equivalent charge in coulombs using Faraday's Law of electrolysis, and is a measure of the total extent of crevice propagation expressed as a charge (Q_W) supported by both external O_2 reduction and internal H^+ reduction. Integration of I_c over the duration of the experiment yields the charge (Q_{O_2}) due to propagation supported by the external reduction of O_2. The difference, $Q_W - Q_{O_2}$, yields the charge due to propagation by the internal reduction of H^+ (Q_H).

Gas chromatography.—[O_2] and [H_2] in the pressure vessel were measured before and after experiments using gas chromatography (GC). Gas samples were taken from the vessel headspace using a home built sampling chamber, and an aliquot extracted for analysis using an air-tight syringe with a Luer Lock (Agilent Technologies) and injected into the GC (Agilent Technologies, Network GC System, 6890N) using N_2 as the carrier gas. The [O_2] was measured using an electron capture detector and [H_2] using a thermal conductivity detector. The GC was calibrated by injecting gas mixtures with known [H_2] and [O_2] from cylinders of certified gas (Praxair).

Scanning electron and optical microscopy (SEM).—SEM was performed with a LEO (Zeiss) 1540XB instrument using either secondary (SE) or backscattered (BSE) electrons, with a beam energy of 10 keV used for all energy dispersive X-ray (EDX) analyses.

A Zeiss SterREO Discovery (V8) optical microscope was used to capture optical images. This technique, alternating with calibrated material grinding steps, was used to produce depth profiles of corrosion damage. The corroded specimen was ground using 600 grit SiC paper, and the resulting reduction in thickness measured using a micrometer. An image was then recorded using a stereo microscope. This procedure was repeated in stages until the microscope revealed a surface free of corrosion (i.e., at the depth of deepest corrosion penetration). A depth profile of the damage was then obtained using image analysis software (Image Pro Plus) to determine the fraction of the surface corroded as a function of grinding depth.

Secondary ion mass spectrometry (SIMS).—Dynamic secondary ion mass spectrometry (SIMS) was employed to obtain compositional information as a function of depth. A modified Cameca IMS-3f ion microscope was used with a 300 nA, 5.5 eV Cs^+ ion beam rastered over a 250 × 250 μm^2 area to collect negative secondary ions within a 150 µm diameter spot for imaging.

Results and Discussion

Figure 3 shows a BSE image of an area of the uncorroded Ti-2 surface. The light spots indicate the presence of Fe, which is a much heavier element than Ti, and the primary impurity in this Ti-2 (Table I). This was confirmed by EDX analyses, which showed that these light spots contain 9.0 to 10.4 wt% (7.8 to 9.1 at%) Fe, although content measured by EDX probably does not reflect its precise composition due to a contribution to the measured Ti from the underlying/surrounding α-Ti matrix. The clustering of white spots suggests Fe was present in intermetallic precipitates, possibly located at grain boundaries. To the extent that such a determination is possible by EDX (resolution ∼1 at%), the dark and gray areas in Figure 3 are 100 at% Ti. The differences in color suggest the darker regions may have been covered by a thicker TiO_2 oxide. Since BSE probes shallower regions than EDX, it is possible that the thin oxides are detectable by BSE. Figure 4 shows a BSE image of a more extended area of the surface. This image captures a series of Fe-containing intermetallic particles.

Figure 5a shows values of I_c, E_c and E_p recorded in an aerated experiment at 150°C. The current, I_c, increased rapidly over the first few hours to a high value (∼3 mA) accompanied by a major decrease in E_c (to ∼ −200 mV). This is the expected signature for the initiation of crevice corrosion and has been discussed in detail previously.[5,9,12] Here, it can be appreciated by comparing E_c to E_p. E_p increased steadily to more positive values as the passive oxide on the planar electrode grew and became more protective. The difference between the two potentials ($E_p - E_c$), Figure 5b, is a measure of the potential difference between the external uncreviced surface and the mouth of the crevice; i.e., a location at the edge of a crevice. Although not an actual measurement of E within the crevice, E_c will be close to the values at actively propagating sites, which are generally located around the periphery of the occluded area. Thus, the difference, $E_p - E_c$, would be expected to be related to I_c. That this is the case can be seen in Figure 5b, each increase/decrease in I_c being accompanied by an increase/decrease in $E_p - E_c$.

The very rapid early increase in I_c suggests an immediate initiation of either a large number of active crevice locations or a small number of very reactive locations. Beyond the first half-day, I_c decreased to a significantly lower value (∼30 µA) and E_c correspondingly increased, although the potential difference, $E_p - E_c$, remained >100 mV, indicating that the crevice, while less active, was not stifled. Since I_c is a measure of only the external support for crevice propagation by O_2 reduction, it is possible that propagation continued at a higher rate, supported by the internal reduction of H^+.

Beyond day 2, a number of additional events occurred, confirming that the crevice was only temporarily dormant. For t > 6 days, $E_p - E_c$, decreased, first rapidly and eventually steadily to <20 mV. This decrease in $E_p - E_c$ was accompanied by a steady decrease in I_c to <100 nA, Figure 6. This very small I_c, accompanied by an effectively insignificant $E_p - E_c$, indicated a complete stifling of crevice propagation. The extreme periodic noise associated with the measured I_c, Figure 6, with minor perturbations in E_c (e.g., between 6.1 and 6.3 days), may reflect locally erratic behavior due to H_2 production in the very small residually active locations and the natural randomness of active corrosion behavior.

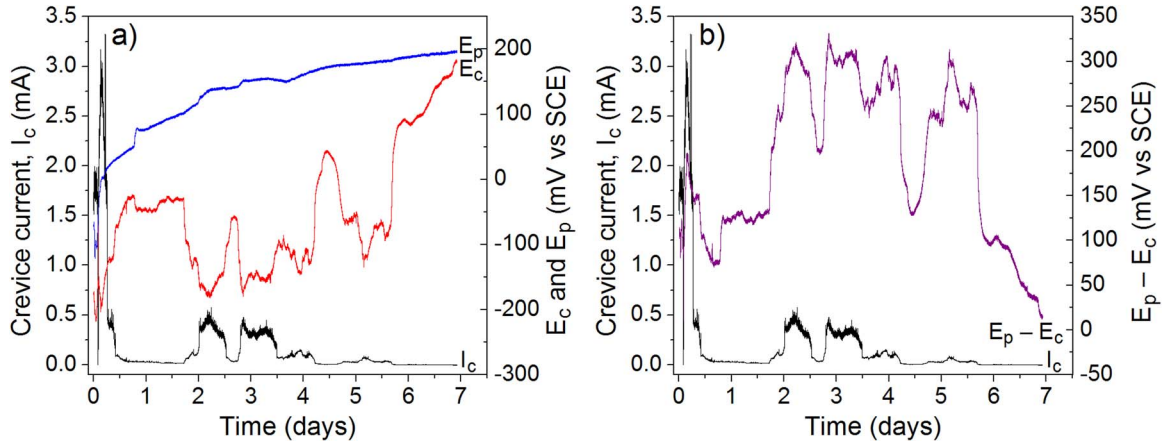

Figure 5. (a) Crevice current (I_c), crevice potential (E_c), and planar potential (E_p) recorded during crevice corrosion of Ti-2 in naturally aerated 1 M NaCl at 150°C; (b) I_c and the calculated $E_p - E_c$ values.

Analyses showed that only 6 vol% of the available O_2 in the cell was consumed in this experiment and that only 20% of the corrosion damage (Q_W) was caused by O_2 consumption on the counter electrode. A repeat experiment yielded similar behavior, only 11 vol% of the O_2 being consumed but with a larger fraction (~40%) of the damage being caused by O_2 reduction. A previous study on a different Ti-2 (containing 0.107 wt% Fe) conducted in 0.27 mol/L NaCl solution also showed the percentage of damage caused by the consumption of O_2 was in the range 20% to 50%.[12] This percentage did not change consistently with [Cl^-] up to 5.0 mol/L, indicating that the electrolyte concentration is not a key feature in the coupling to external crevice support.[15]

While it is possible that extension of this experiment (Figure 5) to longer times could have allowed further active propagation events, this seems unlikely given the progressive decrease in $E_p - E_c$ and the accompanying decrease in I_c. Without a minimum support by O_2 reduction (indicated by the value of I_c), acidification within the crevice cannot be maintained indefinitely, since O_2 reduction coupled to Ti oxidation is ultimately responsible for the development and maintenance of H^+ production within the crevice. Examination of the stoichiometry of H^+ consumption by the internal production of H_2 and H^+ production by Ti^{4+} hydrolysis (to $TiO_2 \cdot xH_2O$) shows they are the same. Therefore, any losses of H^+ due to diffusional escape from the crevice interior, or a failure to produce H^+ (i.e., the incomplete hydrolysis of Ti^{4+}) will result in a pH increase.

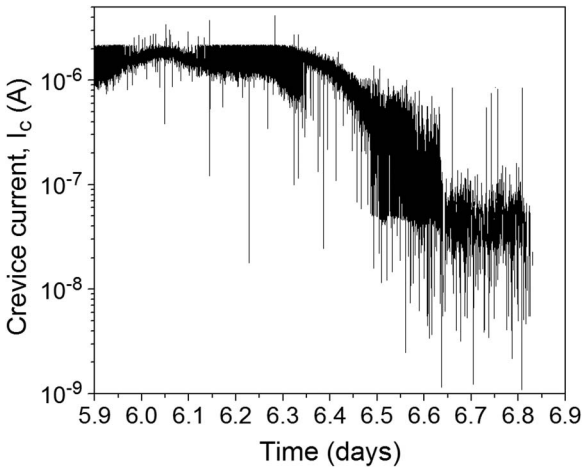

Figure 6. A section of the I_c response (Figure 4) recorded on Ti-2 in naturally aerated 1 M NaCl at 150°C.

Since only 6% of the available O_2 was consumed, it can be concluded that the extent of propagation under these conditions was not controlled by the inventory of available O_2. Similar behavior was observed for intermediate [O_2], with only 23% of the available inventory being consumed when the cell was charged with either a 10% O_2-containing gas or a 3% O_2-containing gas.

Figure 7 shows a corresponding 8-day experiment conducted with a N_2 purge (i.e., a gas containing <0.1 vol% O_2). A number of differences between this low [O_2] and the naturally aerated experiment (Figure 5) can be noted: (i) the value of E_p was lower (~ −50 mV compared to >100 mV), reflecting the influence of the low [O_2] on the passivity of Ti-2; (ii) the difference in the potential, $E_p - E_c$, was considerably smaller and the values of I_c were one to two orders of magnitude smaller; (iii) the initial surge in I_c when crevice corrosion first initiated was relatively minor, a maximum current of only ~0.08 mA being obtained (compared to ~2.8 mA); (iv) while events involving increases in I_c coupled with decreases in E_c were observed, they were relatively minor and superimposed on a steadily decreasing overall current; (v) when the experiment was terminated after 7.75 days, $E_p - E_c$ was effectively constant at ~100 mV and I_c steady at ~6 to 8 μA. This current range is similar to that observed at the higher [O_2] during one of the dormant periods (i.e., from 0.5 to 2 days, Figure 5) which was sufficient to allow the subsequent initiation of additional corrosion events. Consequently, this crevice (at low [O_2]) cannot be considered completely stifled.

In this last experiment, only 26% of the available O_2 (54% in a repeat experiment) was consumed and only 9 to 10% of the corrosion damage attributable to O_2 reduction (11 to 12% in a repeat experiment). Comparison of these values to those observed in the higher [O_2] experiment indicate that when the available [O_2] is low the crevice uses the O_2 to sustain propagation more efficiently, albeit much more slowly, by the internal reduction of H^+. However, since I_c is much lower than at the higher [O_2], the rate of generation of H^+ is considerably lower and propagation would need to be much more localized in order to maintain the critical chemistry required to avoid repassivation.

These results are consistent with the results of our studies on the Ni-Cr-Mo C-22 alloy.[16] In the C-22 experiments, crevice propagation was enforced galvanostatically and the extent and distribution of corrosion damage shown to become more localized as the applied current was reduced, i.e., the current density required to sustain active propagation was maintained by confining corrosion to a smaller number of highly localized sites.

The influence of temperature.—Figure 8a shows the I_c, E_c and E_p values recorded in an experiment conducted in an aerated solution at 120°C over an extended period of 30 days. Comparison to

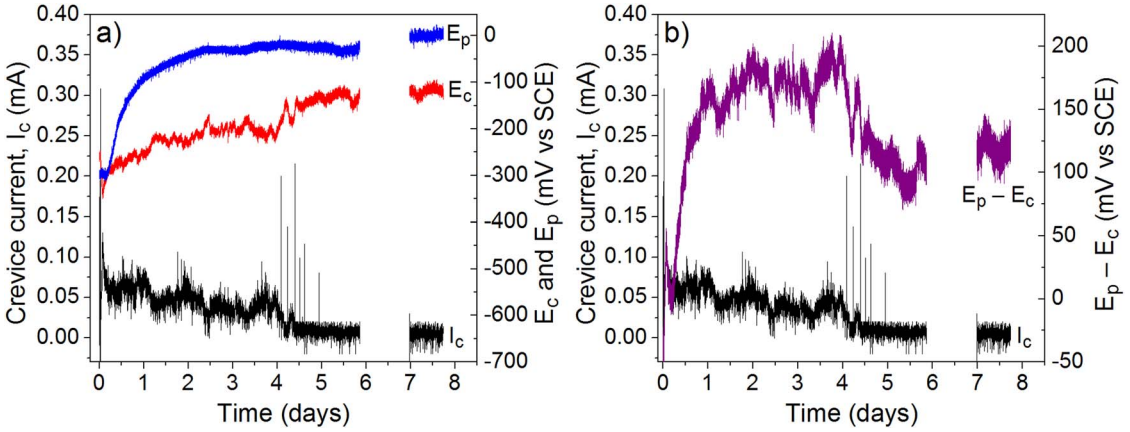

Figure 7. (a) Crevice current (I_c), crevice potential (E_c) and planar potential (E_p) recorded during crevice corrosion of Ti-2 in 1 M NaCl containing a low [O_2] (<0.1 vol%) at 150°C; (b) I_c and the calculated $E_p - E_c$ values. The data between days 6 and 7 were not recorded due to a computer shutdown.

Figure 5 shows that initiation occurs more slowly at 120°C than at 150°C, i.e., a maximum of 0.4 mA (120°C) compared to ∼2.8 mA (150°C). As observed at the higher temperature, a number of discrete events occur. While the maximum I_c values associated with these events are similar to those measured at 150°C, their duration is considerably longer (3 to 4 days compared to 0.5 to 1 day); i.e., the demand for O_2 reduction in support of the event is more persistent. Additionally, while propagation was completely stifled after 7 days at 150°C, propagation at 120°C continued, albeit slowly, for many days after the third event (13 to 16 days). The value of $E_p - E_c$, Figure 8b, was maintained at ∼200 mV, I_c decreasing only slowly from ∼100 μA (16 days) to 20 μA (29 days). Stifling, indicated by the final drop in I_c at 30 days, was only observed when the temperature was allowed to fall to room temperature. A considerable extension of this experiment would have been required to determine whether the very slow decrease in I_c would have eventually led to complete stifling.

While reaction rates are generally increased at higher temperatures, crevice corrosion involves a number of competing and interacting reactions, all of which may depend differently on temperature. During propagation, metal dissolution and oxide formation compete and their relative rates will determine whether the propagation rate increases or decreases. Furthermore, these two processes depend on the rates of different reactions: metal dissolution is driven by both O_2 and H^+ reduction, while the oxide formation rate is determined by metal ion hydrolysis and solubility. Thus, the shorter duration of events at the higher temperature can be attributed to an acceleration of the sequence of reactions, metal dissolution, Ti^{4+} formation, and the deposition of the highly compacted, current-stifling $TiO_2 \cdot xH_2O$. This apparently inverted temperature effect indicates a temperature-accelerated metal dissolution reaction leads to an increase in the rate of formation of stifling deposits, with the overall sequence of reactions controlling the extent of crevice propagation. That this happens more rapidly at 150°C than at 120°C is consistent with previous observations that (over the range 65°C to 85°C) individual corrosion events were stifled more rapidly at higher temperatures[9] and the duration of active crevice corrosion in 0.27 mol/L NaCl at 102°C was up to 10 times greater than observed at 150°C.[11] The alternative explanation, that this difference in behavior at the two temperatures can be attributed to a difference in O_2 solubility, is inconsistent with the observation that the values of I_c are higher at the higher temperature when the O_2 solubility is lower.

Ultimately, the amount of O_2 consumed at 120°C was ∼25% more at the lower temperature ($(Q_{O_2}/Q_W)_{120} = 0.21$, $(Q_{O_2}/Q_W)_{150} = 0.40$) and the overall extent of corrosion damage was considerably larger, 1318 C at 120°C, compared to 463 C at 150°C.

Analyses of corroded surfaces.—Figure 9 shows examples of the optical images recorded on the surfaces after corrosion in naturally aerated and purged ([O_2] < 0.1 vol%) solutions. The locations of corroded sites are visible as light areas where the white $TiO_2 \cdot xH_2O$ corrosion product has accumulated. A large number of initiation sites occur around the edges of the creviced area, the number being greater in the high [O_2] solution, with only very shallow corrosion generally across the surface. No corrosion sites deeper than ∼20 μm are observed beyond the edges of the crevice. Despite this greater extent of

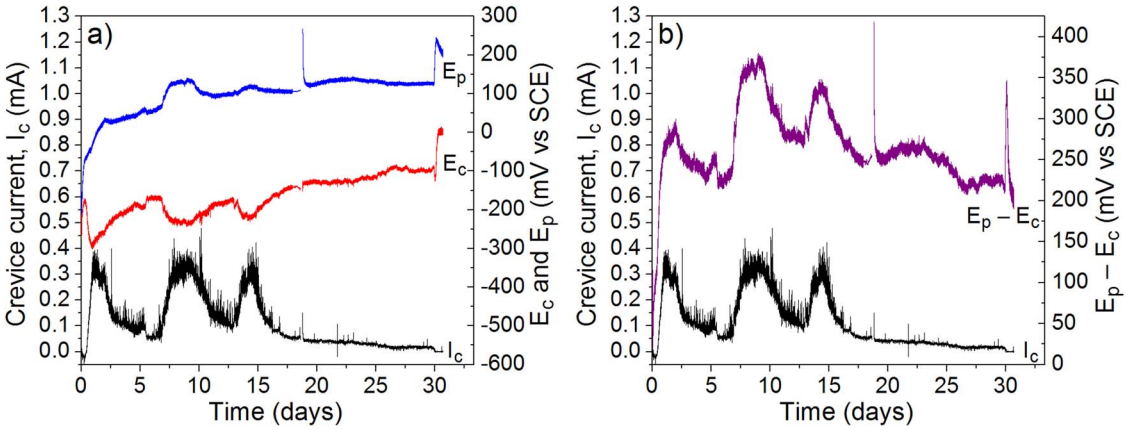

Figure 8. (a) Crevice current (I_c), crevice potential (E_c) and planar potential (E_p) recorded during crevice corrosion of Ti-2 in naturally aerated 1 M NaCl at 120°C; (b) I_c and the calculated $E_p - E_c$ values.

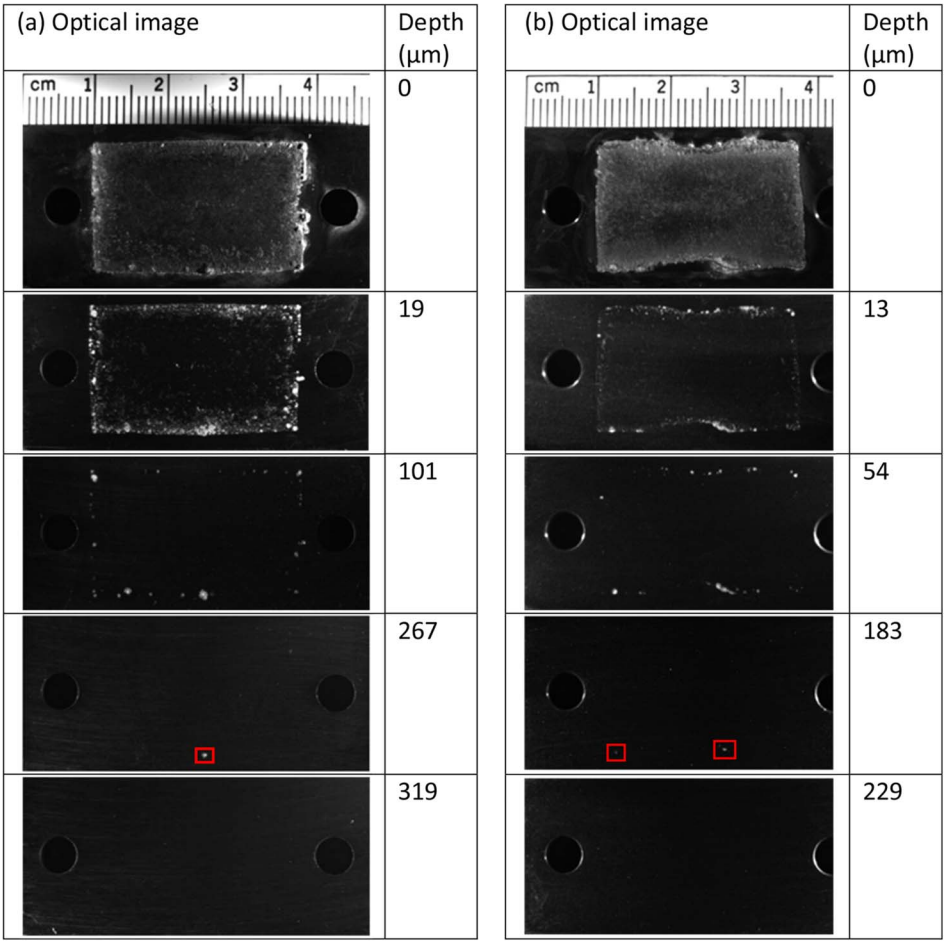

Figure 9. Optical images recorded on Ti-2 crevice corroded in (a) naturally aerated and (b) low (<0.1 vol%) O_2 conditions at 150°C. Light areas are the locations where corrosion has occurred. The depth reported for each image is a measure of the extent of surface grinding prior to recording the image.

initiation at the high $[O_2]$, corrosion propagation to a significant depth is maintained at a small number of locations for both $[O_2]$. These results show that while a greater availability of O_2 may stimulate initiation events, the $[O_2]$ is not dominant in driving the subsequent propagation.

Figure 10 shows corrosion depth profiles (the area of the surface damaged as a function of penetration depth). Irrespective of the $[O_2]$, crevice propagation is highly localized, as indicated by the steep decay in the area corroded as a function of depth. As indicated in the optical images in Figure 9, corrosion propagated deeply at only one or two locations. Previous studies[17] using a different Ti-2 (15 days in 0.27 mol/L NaCl at 95°C) demonstrated a deeper more generally distributed general corrosion front (to a depth of ~200 μm) compared to the 20 to 40 μm observed in the present experiments. The localization of corrosion initiation sites around the edges of the crevice reflects the proximity of those sites to the crevice mouth, which allowed them to more readily couple to O_2 reduction on the external cathode due to the smaller ohmic resistance between these sites and the crevice exterior.

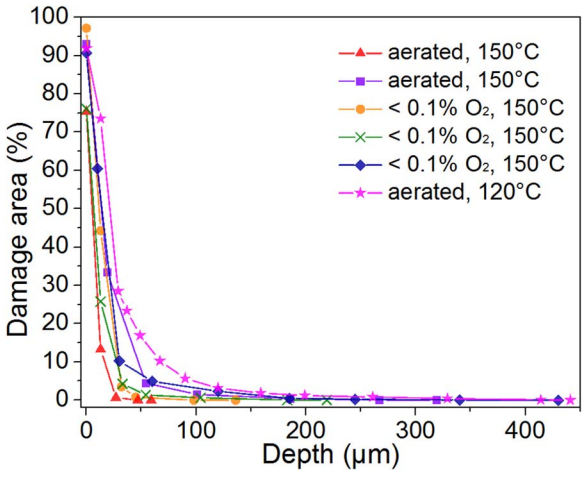

Figure 10. Fraction of the area covered by the crevice former that was damaged by crevice corrosion, as a function of penetration depth for Ti-2 specimens corroded under different conditions.

The optical images (Figure 9) and corrosion depth profiles (Figure 10) show that there is a correlation between the number of deeply corroded sites and the number of large electrochemical events (Figures 5 and 7), suggesting that each deep corrosion site may reflect one of the electrochemical events. The large number of smaller, shallower corrosion sites likely reflects the events occurring in the current surge observed at short exposure times. The depth profiles indicate that the overall extent of corrosion was greater at 120°C, which is expected considering that the duration of the experiment at this temperature was considerably greater than at the higher temperatures, while the degree of localization is similar at both temperatures.

In previous studies, the general spread of corrosion across the creviced surface occurred more readily.[8,17] In those previous studies, individual propagation events were not distinguishable in the I_c/E_c plots, despite the optical images showing some localization in more deeply corroded sites. The slightly broader depth profile observed at 120°C in the present study suggests this tendency for corrosion to spread increases as the temperature decreases. A second feature of the previous studies, in which the accumulation of damage was followed for up to 90 days, is that, while the spread of damage continued with time and O_2 consumption, the maximum penetration depth became independent of time, strongly indicating that the extent of penetration was limited by the stifling effect of the accumulated corrosion product.

Stifling of crevice corrosion under conditions reasonably similar to those used here was previously studied on three different Ti-2 alloys with only slightly different Fe contents (0.042, 0.078 and 0.12 wt%).[12] Repassivation/stifling was enhanced for the highest and lowest Fe-contents, while penetration was deep and widespread at the intermediate Fe level. Microstructurally, decreasing the Fe content leads to an increase in α-Ti grain size. However, an increase leads to the formation of Ti_xFe intermetallic precipitates, inevitably on the grain boundaries.[10,12] Electrochemically, both Fe-containing β-phase and Ti_xFe particles may catalyze H^+ reduction,[5,12] thereby assisting crevice stifling by enhancing cathodic modification. Since the Ti-2 used in this study contains Fe levels at the high end of this range (0.091 wt%) and abundant Ti_xFe intermetallic precipitates are present (Figures 3 and 4), it is likely that crevice stifling was promoted by enhanced cathodic kinetics.

While Ti_xFe intermetallic precipitates can catalyze proton reduction within an active crevice, leading to a suppression of propagation via cathodic modification,[15] they are less stable than the α-Ti matrix. Consequently, besides acting as cathodes they will also be reactive anodes, as illustrated schematically in Figure 11. This combination would make these locations highly reactive, with the cathodic reduction of H^+ counterbalanced by the anodic release of Ti^{3+} and Fe^{2+}. The subsequent conversion of Ti^{3+} to the hydrolysable Ti^{4+} would maintain the local acidity of the site required to sustain propagation until a combination of deposition of $TiO_2 \cdot 2H_2O$ and consumption of available Ti_xFe intermetallic precipitates lead to stifling of propagation at that location. Since the BSE imaging and EDX analyses (Figure 3) show Ti_xFe precipitates tend to occur in clusters, it is likely that these provide the locations for sustained propagation leading to deep localized penetrations.

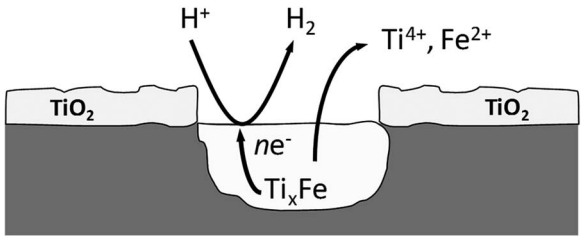

Figure 11. Schematic illustration of proton reduction catalyzed by Ti_xFe precipitates and coupled with the corrosion of the particle itself.

Corrosion at such locations would be expected to be limited not only by the stifling effect of corrosion product accumulation but also by the self-destructive nature of the process. This would explain the limited duration of the major events observed in the I_c/E_c plots. However, except in the experiment at 150°C under aerated conditions, the evidence for complete stifling is elusive, the very small currents (I_c in the range 5 μA to 10 μA) still being able to maintain active occluded sites.

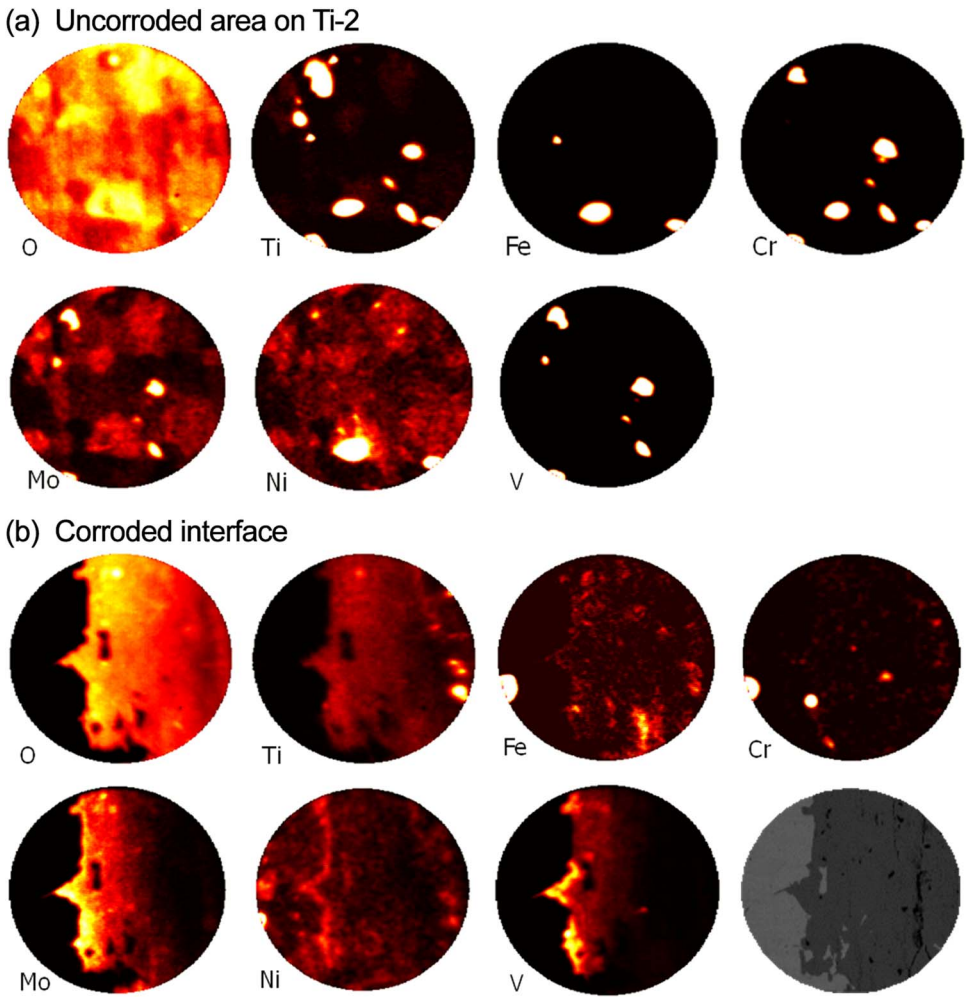

Figure 12. SIMS images of (a) uncorroded Ti-2 and (b) the interface between the Ti-2 and the corrosion product in cross section (after corrosion at 150°C in aerated solution). The last image in (b) is the corresponding BSE image of the area analyzed by SIMS. The diameter of the surface area encompassed by the images is 150 μm.

SIMS analysis.—A SIMS analysis of the uncorroded metal, Figure 12, confirms the presence of Fe in intermetallic precipitates, as indicated by the EDX analyses. In addition, the minor impurities Cr, V, Mo and Ni also tend to localize in these particles. These impurities may increase the susceptibility of those precipitates to corrosion, and, at least in the case of Ni,[5,7] their ability to catalyze H^+ reduction. The brightness of the Fe spots associated with these particles conceals any finer distribution of this element, and the brightness of the Ti signal in these locations is due to the preferential sputtering of these particles in the beam.

The SIMS images recorded on a cross section location at the boundary between the corrosion product deposit and the underlying metal clearly identify the interface between the alloy (left) and the corrosion product (right), Figure 12b. The distribution of Fe throughout the corrosion product supports the argument that the Ti_xFe intermetallic particles are unstable and are anodically dissolved during crevice propagation, with the dissolved Fe^{2+} subsequently co-precipitated with the Ti^{4+} in the $TiO_2 \cdot xH_2O$ deposit. There also appears to be some enrichment of Mo, Ni and V at the corroded interface. This could be a factor in enhancing the stifling of propagation, since V, and especially Mo, are known to form protective surface layers on Ti alloys[18] and Mo has been demonstrated to accumulate locally in the form of protective molybdate on the surfaces of crevice corroding Ni-Cr-Mo alloys.[19]

While Mo and V are distributed throughout the oxide close to the corroded interface, the Ni is concentrated at the interface itself. It has been long suspected that Ni either accumulates on the surface as the surrounding Ti corrodes[13,14,20,21] or that it dissolves and subsequently redeposits on the surface in metallic form[22] where it can catalyze the reduction of H^+ to stifle propagation by the cathodic modification mechanism.[5]

This behavior can be compared to that of Grade-12 titanium (Ti-12), to which Mo and Ni are deliberately added, the latter to promote stifling by cathodic modification. While considerably more resistant to crevice corrosion than this Ti-2, in similar experiments Ti-12 experienced generally shallow corrosion with a modest number of small but deeply corroded locations.[18] Similar I_c/E_c events were observed, lasting 0.5 to 1 day at 120°C and 2 to 3 days at 95°C; i.e., as observed in the present study, stifling was more rapidly enforced at the higher temperature. In addition, 97% of crevice propagation on Ti-12 was supported internally by H^+ reduction, which is similar to the 88% to 91% observed in this study. Finally, SIMS analyses of cross sections of corroded Ti-12 demonstrated a similar, but more marked accumulation of Mo and Ni at the corroded interface. These similarities suggest that the Ti-2 used in this study is acting like a less resistant imitation of Ti-12, with corrosion limited by the accumulation of impurities at the corroded interface leading to a combination of cathodic modification and stifling by corrosion product accumulations at active locations.

Conclusions

- The influence of O_2 concentration and temperature on the propagation of crevice corrosion on commercially available Grade-2 titanium (Ti-2) was investigated in 1.0 mol/L NaCl solutions.
- Irrespective of the temperature and O_2 concentration, propagation was stifled after $\leq$50% of the available O_2 had been consumed. This was attributed to the formation of compact $TiO_2 \cdot xH_2O$ deposits within actively propagating sites.
- This stifling process may also be aided by the accumulation of minor alloy impurities (e.g., Fe, V. Mo) at these locations.
- As a consequence of corrosion product deposition, the extent of corrosion damage is less at higher (150°C) than lower (120°C) temperatures. While active corrosion initially proceeds more rapidly at the higher temperature, it is also more rapidly stifled, leading to the accumulation of less corrosion damage.
- The majority of the propagation was supported by the internal reduction of protons and caused relatively deep penetrations at a small number of sites. This localization was caused by the corrosion of Ti_xFe intermetallic particles, which are both anodically reactive and catalytic cathodes for H^+ reduction. This enables them to both create and consume the protons required to maintain internally-supported crevice propagation.
- While stifling occurred, complete repassivation of active sites was difficult to achieve and propagation may continue for long periods of time by maintaining high current densities at highly localized sites, providing the supply of O_2 is maintained.
- These results show that the damage likely to be accumulated by Ti nuclear waste containers cannot be straightforwardly predicted using a model which simply accounts for the consumption of oxygen in a deep geological repository (DGR).

Acknowledgment

This project was funded by AMEC Foster Wheeler under contract to the Nuclear Decommissioning Authority (NDA), Radioactive Waste Management Directive (RWMD), Didcot, UK.

References

1. F. King and C. Padovani, *Corros. Sci. Eng. Technol.*, **46**, 82 (2011).
2. F. Hua, K. Mon, P. Pasupathi, G. Gordon, and D. W. Shoesmith, in *Corrosion 2004*, Paper No. 04689, NACE International, Houston, TX (2004).
3. F. Hua, K. Mon, P. Pasupathi, G. Gordon, and D. W. Shoesmith, in *Corrosion 2005*, Paper No. 05582, NACE International, Houston, TX (2005).
4. D. W. Shoesmith, *Corrosion*, **62**, 703 (2006).
5. X. He, thesis, Ph.D. Thesis, the University of Western Ontario, London, ON (2003).
6. E. J. Kelly, *J. Electrochem. Soc.*, **123**, 162 (1976).
7. J. Been and J. S. Grauman, in *Uhlig's Corrosion Handbook*, R. W. Revie, Editor, vol. 3, p. 861, John Wiley & Sons, Inc, Hoboken, NJ (2011).
8. L. Yan, thesis, Ph.D. Thesis, the University of Western Ontario, London, ON (2007).
9. X. He, J. J. Noël, and D. W. Shoesmith, *J. Electrochem. Soc.*, **149**, B440 (2002).
10. J. J. Noël, *thesis*, The University of Manitoba. Winnipeg, MB (1999).
11. B. M. Ikeda, M. G. Bailey, M. J. Quinn, and D. W. Shoesmith, in *Innovation and Technology Transfer for Corrosion Control, 11th International Corrosion Congress*, vol. 5, p. 5, Florence, Italy (1990).
12. X. He, J. J. Noël, and D. W. Shoesmith, *Corrosion*, **60**, 378 (2004).
13. M. Stern and H. Wissenberg, *J. Electrochem. Soc*, **106**, 759 (1959).
14. E. van der Lingen and H. de Villiers Steyn, in *Proc. Titanium Applications Conference*, p. 450–461, Titanium Development Association, Boulder, CO (1994).
15. L. Yan, J. J. Noël, and D. W. Shoesmith, *Electrochim. Acta*, **56**, 1810 (2011).
16. P. Jakupi, J. J. Noël, and D. W. Shoesmith, *Corros. Sci.*, **54**, 260 (2012).
17. X. He, J. J. Noël, and D. W. Shoesmith, *Corros. Sci.*, **47**, 1177 (2005).
18. X. He, J. J. Noël, and D. W. Shoesmith, *J. ASTM Int.*, **5**, 1 (2008).
19. N. Ebrahimi, P. Jakupi, J. J. Noël, and D. W. Shoesmith, *Corrosion*, **71**, 1441 (2015).
20. N. D. Tomashov, G. P. Chernova, Y. S. Ruscol, and G. A. Ayuyan, *Electrochim. Acta*, **19**, 158 (1974).
21. R. S. Glass, *Electrochim. Acta*, **28**, 1507 (1983).
22. A. J. Sedriks, J. A. S. Green, and D. L. Novak, *Corrosion*, **28**, 137 (1972).